Journal of Power Sources 195 (2010) 7259–7263

Contents lists available at ScienceDirect

Journal of Power Sources

journal homepage: www.elsevier.com/locate/jpowsour

Short communication

Electrochemical characterization of MnOOH–carbon nanocomposite cathodes for metal-air batteries: Impacts of dispersion and interfacial contact

Chi-Chang Hu[a,*], Shi-Cyuan Liao[b], Kuo-Hsin Chang[a,b], Yi-Lin Yang[b], Kuo-Min Lin[a]

[a] Department of Chemical Engineering, National Tsing Hua University, Hsin-Chu 30013, Taiwan
[b] Department of Chemical Engineering, National Chung Cheng University, Chia-Yi 621, Taiwan

ARTICLE INFO

Article history:
Received 14 December 2009
Received in revised form 10 May 2010
Accepted 11 May 2010
Available online 19 May 2010

Keywords:
Manganese hydroxide nanowires
Oxygen reduction
Composite cathode
Oxide dispersion
Interfacial contact

ABSTRACT

The importance of MnOOH dispersion and interfacial contact between MnOOH nanowires and carbon black for the cathode of metal-air batteries has been clearly demonstrated from the textural, voltammetric, and electrochemical impedance spectroscopic (EIS) analyses. In comparing with the physically mixed composite, the MnOOH nanowires/XC-72 composite co-precipitated by hydrothermal synthesis shows much better performances of oxygen reduction in 1 M KOH, which is attributed to the higher active surface area resulting from the better dispersion of MnOOH and the smooth electron pathways resulting from the higher interfacial contact surface area between oxide and carbon nanoparticles within the hydrothermally co-precipitated MnOOH/XC-72 nanocomposites. The absence of diffusion responses in the low-frequency range of EIS spectra reveals no/minor oxygen-diffusion effect at low overpotentials ($E \geq -0.3$ V *vs.* Ag/AgCl).

1. Introduction

Due to the important applications of metal-air batteries and fuel cells, the oxygen reduction reaction (ORR) aiming at 4-electron transfer has been extensively studied [1–6]. The kinetics of ORR was found to strongly depend on the constituents of electrodes, such as the catalyst layer [7,8], current collector [9,10], and hydrophobic gas-distribution/diffusion membrane [11,12]. Moreover, developing carbon-based electrodes containing catalysts for achieving 4-electron transfer is one of the most important researches in the ORR [7,13,14] although the high-cost Pt has been recognized as the best electrocatalyst in acidic media [15].

Transition metal oxides, such as Ni/Ni-based oxides [16,17] and Mn/Mn-based oxides [3,7] were developed to achieve the purpose of low costly, highly active electrocatalysts for the ORR. These electroactive materials in various nanostructures, such as nanoparticles [18] and nanowires [19], are usually found to advance their reactivity. Hence, several 3D mesoporous architectures were designed to produce gas-depolarized cathodes by simultaneously enhancing the oxygen transfer rate, the three-phase reaction zone, and the electronic conductivity. However, most studies ignore the importance of interfacial contact between electrocatalysts and carbon support in the catalyst layer, which is a strong function of the electrocatalyst dispersion, although the interface is a part of the electron pathways and the real active surface area of the catalyst layer strongly depends on the dispersion degree of electrocatalysts. Accordingly, a poor interfacial contact between electrocatalysts and carbons resulting from poor dispersion of electrocatalysts will significantly reduce the electron-hopping rate and may become the bottleneck step in the high-rate application, even though the activity of electrocatalysts is excellent. Therefore, the contact resistance at the electrocatalyst–carbon interface as well as the dispersion of active materials within the catalyst layer has to be carefully considered in developing/designing the air-cathodes.

In this work, MnOOH nanowires/carbon composites are employed as the model cathode. Nanocomposites prepared by hydrothermal co-precipitation and physical mixing processes are compared to demonstrate the importance of interfacial contact between MnOOH nanowires and carbon as well as the dispersion of MnOOH nanowires within the catalyst layer. Although air-cathodes of MnO_x/carbon composites have been studied previously [20], to the best of our knowledge, this work is the first report successfully demonstrating these key technology concepts in developing carbon-based air-cathodes. The influences of real active surface area and interfacial contact on the ORR at the MnOOH nanowires/carbon cathodes can be clearly evaluated by the microstructure and electrochemical analyses. A reliable equivalent-circuit model for the ORR on the air-cathodes is therefore established, which is applicable to various ORR cathodes of other fuel cell systems.

* Corresponding author at: Department of Chemical Engineering, National Tsing Hua University, 101, Section 2, Kuang-Fu Road, Hsin-Chu 30013, Taiwan.
Tel.: +886 3 573 6027; fax: +886 3 573 6027.
E-mail address: cchu@che.nthu.edu.tw (C.-C. Hu).

0378-7753/$ – see front matter © 2010 Elsevier B.V. All rights reserved.
doi:10.1016/j.jpowsour.2010.05.021

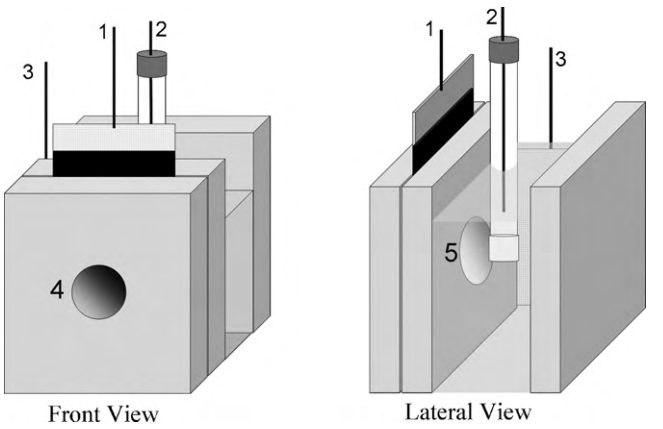

Fig. 1. The setup of electrochemical measurements for the hot-pressed air-cathodes consisting of a MnOOH/XC-72 layer and a gas-diffusion layer; 1: working electrode; 2: reference electrode; 3: counter electrode; 4: hole opened to the air; 5: hole opened to the electrolyte; the hole exposed surface area to the air and electrolyte is equal to 3.14 cm^2.

2. Experimental

MnOOH nanowires were synthesized by a low-temperature hydrothermal method according to our previous work [21]. For preparing co-precipitated MnOOH–carbon composites (c-MnOOH–C), carbon black (Vulcan XC-72) powders were added in a solution containing 10 mM $K_2S_2O_8$ and 20 mM $Mn(CH_3COO)_2{\cdot}4H_2O$ and stirred for 6 h to obtain a well-suspended solution, then, followed the same steps for preparing MnOOH. The precipitates were obtained by a centrifuge and washed with deionized water several times until pH ~ 7. The mass ratio of XC-72/MnOOH is confirmed to be 3 and all precipitates were dried in a reduced-pressure oven at room temperature overnight for material analysis.

For preparing the physically mixed composite (denoted as p-MnOOH–C), MnOOH, XC-72, and PTFE in the 20:60:20 mass ratio were ground for 30 min. Few drops of isopropyl alcohol (IPA) were added into the mixture to form a cold-rolled paste. Similarly, c-MnOOH–C powders were mixed with 20 wt% PTFE and ground for 30 min and added with IPA to form the paste. A 40 mm × 40 mm electrocatalyst layer was punched from the paste. A stainless steel grid was hot-pressed between a gas-diffusion layer and an electrocatalyst layer at 80 °C under 100 kgf cm^{-2} for 15 min to form the cathode.

The morphologies and microstructures of MnOOH nanowires and composites were examined using a field-emission scanning electron microscope (FE-SEM, Hitachi S4800 type I) and a field-emission transmission electron microscope (FE-TEM, Philips Tecnai). Fig. 1 shows the setup of electrochemical measurements in this work, where the gas-diffusion layer and MnOOH/XC-72 layer of the hot-pressed cathode were directly exposed to the air and the 1 M KOH electrolyte, respectively. The electrochemical characteristics were examined by an electrochemical analyzer, CHI 633A (CH Instruments, USA) in a two-compartment cell. The impedance spectrum analyzer, IM6 (ZAHNER), with the Thales software was employed to measure and analyze the EIS data. The potential amplitude of ac is 10 mV meanwhile its frequency region is from 0.1 to 20,000 Hz. An Ag/AgCl electrode (Argenthal, 3 M KCl, 0.207 V *vs.* SHE at 25 °C) was used as the reference and a large piece of platinum

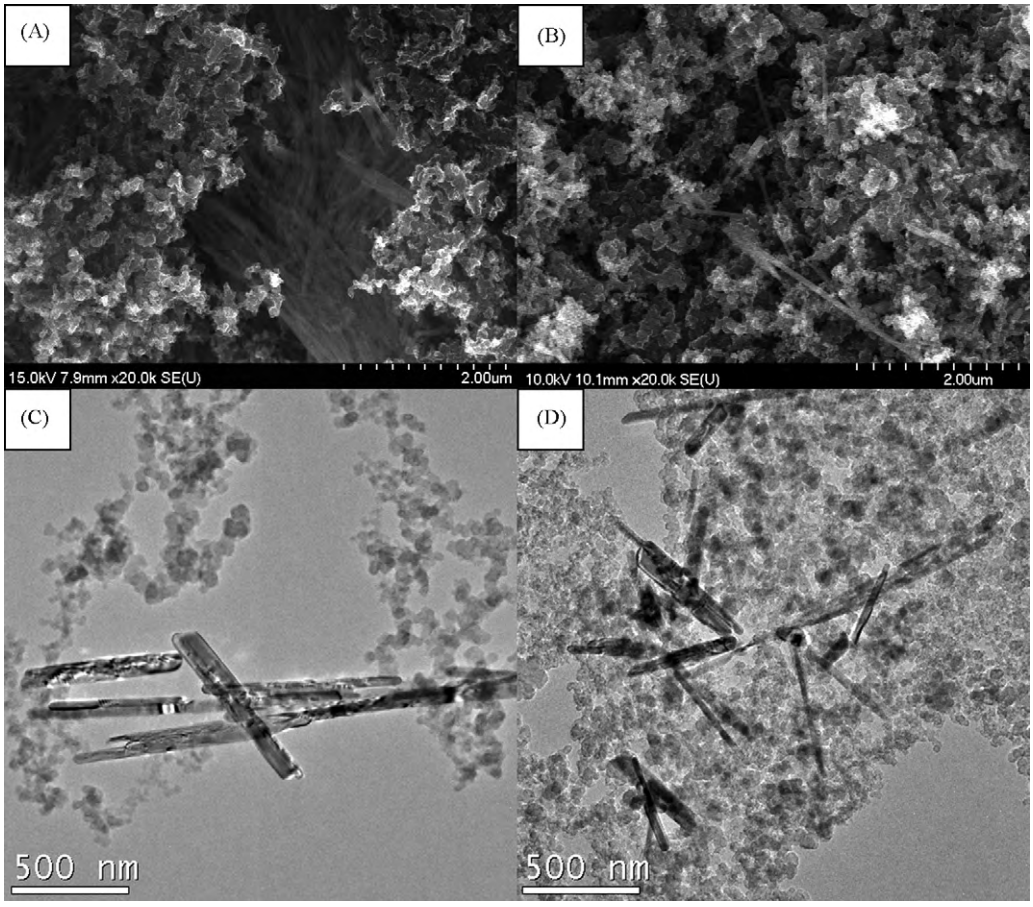

Fig. 2. (A and B) FE-SEM and (C and D) FE-TEM images of (A and C) p-MnOOH–C and (B and D) c-MnOOH–C composites.

gauze was employed as the counter electrode. A Luggin capillary was used to minimize errors due to *iR* drop in the electrolytes. All solutions used in this work were prepared with 18 MΩ cm water produced by a reagent water system (Milli-Q SP, Japan).

3. Results and discussion

The difference at the MnOOH/XC-72 interface between p-MnOOH–C and c-MnOOH–C is clearly visible in the SEM and TEM images (see Fig. 2). Very long nanowires of MnOOH and massive aggregates of XC-72 particles are found in Fig. 2A and B, while aggregates of MnOOH nanowires are visible for p-MnOOH–C, suggesting poor MnOOH dispersion. The morphologies of MnOOH nanowires in p-MnOOH–C and c-MnOOH–C are similar, indicating that the formation and growth of single-crystalline MnOOH nanowires are not significantly influenced by coexistence of XC72 powders and Mn precursors. The single-crystalline structure of MnOOH nanowires has been previously confirmed by the SAED pattern [21]. All the above results indicate that the low-temperature hydrothermal synthesis is a reliable method for preparing MnOOH nanowires [21]. From a comparison of Fig. 2C and D, the dispersion of MnOOH nanowires within XC-72 particles (20–50 nm in diameter) for p-MnOOH–C is worse than that for c-MnOOH–C. The highly interfacial contact between MnOOH nanowires and XC-72 is clearly found on c-MnOOH–C from the TEM image, which is poor on p-MnOOH–C. The above results reveal that our proposed synthesis procedure, hydrothermal co-precipitation of MnOOH and XC-72, is an effective method for preparing MnOOH–C nanocomposites with good dispersion of active materials.

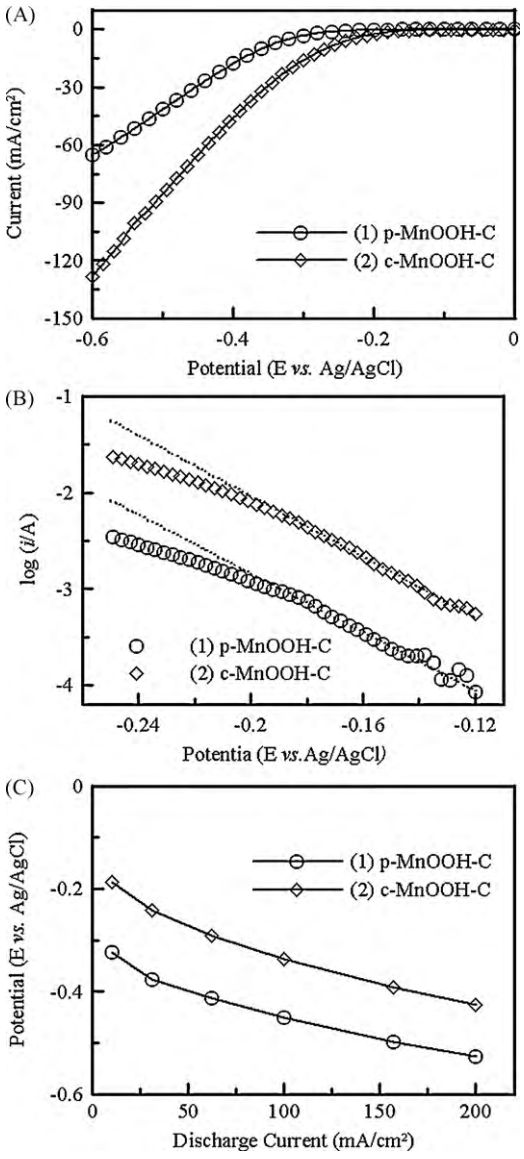

Fig. 3. (A) LSV measured at 5 mV s^{-1} from 0 to −0.6 V, (B) log(i) − E measured at 0.5 mV s^{-1} from 0 to −0.25 V, and (C) steady-state discharge curves of (1) p-MnOOH–C and (2) c-MnOOH–C composites in 1 M KOH; the gas-diffusion layer and MnOOH/XC-72 layer of hot-pressed cathodes were directly exposed to the air and the 1 M KOH electrolyte, respectively.

Table 1
The best-fitting values of equivalent-circuit elements in Fig. 4C for the impedance data shown in Fig. 4A and B.

Composite	p-MnOOH–C		c-MnOOH–C	
E_{OCP} (V)	−0.089		0.005	
E_{biased} (V)	E_{OCP}	−0.3	E_{OCP}	−0.3
R_s (mΩ)	68.87	71.27	52.01	52.92
R_{ect} (Ω)	328.7	0.430	65.94	0.053
T_1 (C_{dl}) (mF cm^{-2})$^{\alpha 1}$	10.35	12.86	48.34	46.38
α_1	0.939	0.907	0.727	0.810
R_{iet} (Ω)	8.805	2.483	0.566	0.256
T_2 (C_i) (mF cm^{-2})$^{\alpha 2}$	5.827	6.993	22.74	36.55
α_2	0.849	0.954	0.772	0.803

Effects of the MnOOH/XC-72 interfacial contact and MnOOH dispersion on the cathode performance are clearly found in Fig. 3. From Fig. 3A, the decomposition potentials of the ORR (defined as the potential where voltammetric current = 1 mA) are equal to −0.250 and −0.165 V for p-MnOOH–C and c-MnOOH–C, respectively. The two tafel plots in Fig. 3B are parallel in the whole potential region of investigation while the current density on curve 2 is about one-order higher than that on curve 1. These results suggest the same ORR mechanism, attributable to the same electrocatalyst on both nanocomposites. The curvature around −0.18 V is not attributable to the oxygen-diffusion issue because the diffusion effect should occur at similar current densities (but not similar electrode potentials). The difference in electrode potentials measured at the same applied currents in the relatively high current density region (> 10 mA cm^{-2}) is almost constant (see Fig. 3C), further emphasizing the importance of MnOOH/carbon interfacial contact and MnOOH dispersion.

Effects of the above two factors on the ORR rate at air-cathodes are quantitatively evaluated by the EIS analysis through establishing and fitting a reliable equivalent-circuit model. Typical EIS spectra, measured at the open-circuit potential (E_{OCP}) and −0.3 V on p-MnOOH–C and c-MnOOH–C, and the corresponding equivalent-circuit model are shown in Fig. 4. From Fig. 4A, the ORR on the air-cathode at E_{OCP} is not under diffusion control because the net current of ORR is zero. The 45°-like responses in the low-frequency region on both curves are not attributable to the oxygen-diffusion effect. Such responses correspond to an incomplete semi-circle arc for the faradaic ORR. These statements are supported by the absence of 45°-like responses in the low-frequency region of the EIS spectra measured at −0.3 V for both air-cathodes (i.e., Fig. 4B). Since the measured steady current at −0.3 V is about 28 mA for c-MnOOH–C, the absence of the 45°-like responses at the low-frequency end reveals no/minor oxygen-diffusion effect in this relatively low overpotential region. Hence, it is not reasonable to put the diffusion element (W) in the equivalent-circuit model for data fitting in the potential region of investigation (see Table 1). Note that when the air-cathodes are polarized at more negative potentials, the oxygen-diffusion responses in the low-frequency region should be visible, and the oxygen-diffusion effect becomes significant although this work does not focus on this phenomenon.

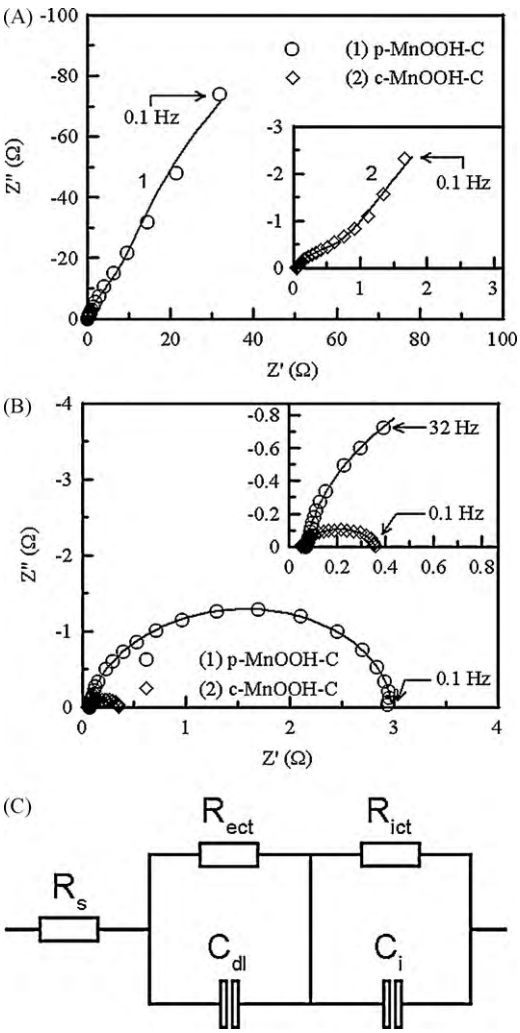

Fig. 4. Electrochemical impedance spectra measured at (A) E_{OCP} and (B) −0.3 V for (1) p-MnOOH–C and (2) c-MnOOH–C composites in 1 M KOH. (C) The equivalent-circuit model of MnOOH–C composites for oxygen reduction.

In Fig. 4A and B, the solid lines represent the best-fit curves in terms of the equivalent circuits in Fig. 4C. The good fitting indicates that the equivalent-circuit model reasonably represents the electrochemical processes at both MnOOH–C cathodes. The best-fit values of the equivalent-circuit elements are listed in Table 1. The analysis of $Z(\omega)$ for both air-cathodes in the potential region of interest is based on the following equations:

$$Z(\omega) = R_S + Z_{3P}(\omega) + Z_I(\omega) \quad (1)$$

$$\frac{1}{Z_{3P}(\omega)} = \frac{1}{R_{ect}} + j\omega C_{dl} \quad (2)$$

$$\frac{1}{Z_I(\omega)} = \frac{1}{R_{ie}} + j\omega C_i \quad (3)$$

where ω, R_S, Z_{3P}, Z_I, R_{ect}, R_{ie}, C_{dl}, and C_i are the angular frequency, solution resistance, impedance of the three-phase reaction zone, impedance of the MnOOH/XC-72 interfacial contact, electrochemical charge-transfer resistance at the three-phase reaction zone, interfacial electron-hopping resistance at the MnOOH/XC-72 contact, double-layer capacitance in the three-phase reaction zone, and the interfacial contact capacitance between MnOOH and XC-72, respectively. Due to the porous nature, a constant phase element (CPE), T, reasonably replaces the capacitor elements. A CPE is usually defined as $1/T(j\omega)^{\alpha}$, where T is a constant with dimensions $(\mathrm{mF\,cm^{-2}})^{\alpha}$, which has been associated with the roughness of the electrode surfaces or the redox kinetics of active materials, causing the rotation of the impedance semi-circles by an angle of $(1-\alpha)$ 90° [22]. Based on the above analyses, Z_{3P} and Z_I can be employed to describe the MnOOH dispersion within the composites and the interface contact between MnOOH and XC-72.

In Table 1, the bulk solution resistance, R_S, is very low and approximately independent of the biased potentials, which is a function of the distance between the Luggin capillary tip and the cathode [23]. The electrochemical charge-transfer resistance, R_{ect}, in parallel with a double-layer capacitor of the three-phase reaction zone, C_{dl} (T_1), reasonably decreases with a higher overpotential. Note the much larger three-phase reaction zone capacitance (T_1) of c-MnOOH–C as well as the much lower R_{ect} of c-MnOOH–C in comparison with p-MnOOH–C at E_{OCP} and −0.3 V. The former result indicates a larger three-phase reaction zone of c-MnOOH–C resulting from better dispersion of MnOOH. This effect significantly reduces the electrochemical charge-transfer resistance, R_{ect}, of c-MnOOH–C due to its higher active surface area, and enhances the ORR rate, consistent with the results obtained in Fig. 3. The well dispersion of MnOOH within XC-72 and the larger contact surface area at the MnOOH/XC-72 interface will increase the electron pathways for the ORR since 4-electron-transfer ORR is simultaneously catalyzed by the carbon nanoparticles and MnOOH nanowires [2–4,24]. Consequently, the interfacial electron-hopping resistance, R_{ie}, in parallel with an interfacial capacitor at the MnOOH/XC-72 interface, C_i (T_2), for c-MnOOH–C is much lower than that for p-MnOOH–C. Similarly, the more interfacial contact surface areas on c-MnOOH–C shows a much higher T_2 value in comparison with p-MnOOH–C, further revealing the better interfacial contact between MnOOH and XC-72 through a chemical route (hydrothermal co-precipitation in this work). Based on this section, the electrochemical impedance analyses in this work not only precisely show the better dispersion of MnOOH but also demonstrate the larger interfacial contact of the hydrothermal co-precipitated nanocomposites, which are concluded to be two of the key factors influencing the performance of MnOOH/XC-72 cathodes for the ORR.

4. Conclusions

From the SEM and TEM images, hydrothermal co-precipitation significantly improves the MnOOH dispersion and the interfacial contact between MnOOH nanowires and XC-72 nanoparticles in comparing with the physically mixed composite. Based on the voltammetric and EIS analyses, better MnOOH dispersion and higher MnOOH/XC-72 interfacial contact enhances the electrochemical activity of c-MnOOH–C for the ORR because of larger active surface area and more electron pathways of the resultant nanocomposite prepared by the hydrothermal co-precipitation. The absence of 45°-like responses at the low-frequency end of the EIS spectra measured at −0.3 V reveals no/minor oxygen-diffusion effect in the relatively low overpotential region.

Acknowledgments

The financial support of this work, by the National Science Council of ROC (NSC 98-3114-E-007-011) and the boost program of NTHU, is gratefully acknowledged.

References

[1] J.S. Spendelow, A. Wieckowski, Phys. Chem. Chem. Phys. 9 (2007) 2654.
[2] M.S. El-Deab, T. Ohsaka, J. Electrochem. Soc. 155 (2008) D14.
[3] L. Mao, T. Sotomura, K. Nakatsu, N. Koshiba, D. Zhang, T. Ohsaka, J. Electrochem. Soc. 149 (2002) A504.
[4] L. Mao, D. Zhang, T. Sotomura, K. Nakatsu, N. Koshiba, T. Ohsaka, Electrochim. Acta 48 (2003) 1015.

[5] Y. Takasu, N. Yoshinaga, W. Sugimoto, Electrochem. Commun. 10 (2008) 668.
[6] B. Klapste, J. Vondrak, J. Velicka, Electrochim. Acta 47 (2002) 2365.
[7] Y.G. Wang, L. Cheng, F. Li, H.M. Xiong, Y.Y. Xia, Chem. Mater. 19 (2007) 2095.
[8] R. Kou, Y. Shao, D. Wang, M.H. Engelhard, J.H. Kwak, J. Wang, V.V. Viswanathan, C. Wang, Y. Lin, Y. Wang, I.A. Aksay, J. Liu, Electrochem. Commun. 11 (2009) 954.
[9] D. Chartouni, N. Kuriyama, T. Kiyobayashi, J. Chen, J. Alloys Compd. 330 (2002) 766.
[10] C.C. Yang, J. Hydrogen Energy 29 (2004) 135.
[11] G.Q. Zhang, X.G. Zhang, Y.G. Wang, Carbon 42 (2004) 3097.
[12] G.Q. Zhang, X.G. Zhang, Electrochim. Acta 49 (2004) 873.
[13] C.Y. Wu, P.W. Wu, P. Lin, Y.Y. Li, Y.M. Lin, J. Electrochem. Soc. 154 (2007) B1059.
[14] D. Qu, Carbon 45 (2007) 1296.
[15] K. Kinoshita, Electrochemical Oxygen Technology, Wiley, New York, 1992.
[16] S. Mukerjee, S. Srinivasan, J. Electroanal. Chem. 357 (1993) 201.
[17] F.H.B. Lima, J.R.C. Salgado, E.R. Gonzalez, E.A. Ticianelli, J. Electrochem. Soc. 154 (2007) A369.
[18] M.L. Calegaro, F.H.B. Lima, E.A. Ticianelli, J. Power Sources 158 (2006) 735.
[19] F.Y. Cheng, J. Shen, W.Q. Ji, Z.L. Tao, J. Chen, Appl. Mater. Interf. 1 (2009) 460.
[20] P. Zoltowski, D.M. Drazic, L. Vorkapic, J. Appl. Electrochem. 3 (1973) 271.
[21] C.C. Hu, Y.T. Wu, K.H. Chang, Chem. Mater. 20 (2008) 2890.
[22] E. Barsoukov, J.R. Macdonald (Eds.), Impedance Spectroscopy: Theory, Experiment, and Applications, 2nd ed., Wiley-Interscience, Hoboken, NJ, 2005.
[23] C.C. Hu, C.H. Chu, J. Electroanal. Chem. 503 (2000) 105.
[24] C.W. Lee, K. Sathiyanarayanan, S.W. Eoma, H.S. Kim, M.S. Yun, J. Power Sources 159 (2006) 1474.